

Article

Reduction Characteristics of Carbon-Containing REE–Nb–Fe Ore Pellets

Bo Zhang ^{1,2,*}, Yong Fan ^{3,4,*} , Chengjun Liu ^{1,2}, Yun Ye ^{1,2} and Maofa Jiang ^{1,2}

¹ School of Metallurgy, Northeastern University, Shenyang 110819, China; liucj@smm.neu.edu.cn (C.L.); 20152529@stu.neu.edu.cn (Y.Y.); jiangmf@smm.neu.edu.cn (M.J.)

² Key Laboratory for Ecological Metallurgy of Multimetallic Ores (Ministry of Education), Northeastern University, Shenyang 110819, China

³ Institute of Multidisciplinary Research for Advanced Materials, Tohoku University, Sendai 980-8577, Japan

⁴ Institute of Iron and Steel Technology, TU Bergakademie Freiberg, 09599 Freiberg, Germany

* Correspondence: zhangbo@smm.neu.edu.cn (B.Z.); Yong.Fan@extern.tu-freiberg.de (Y.F.)

Received: 29 December 2017; Accepted: 19 March 2018; Published: 23 March 2018



Abstract: To separate and recover the valuable metals from low-grade REE (rare earth elements)–Nb–Fe ore in China, the reduction characteristics of carbon-containing REE–Nb–Fe ore pellets, including mineral phase variation, reduction degree, and reaction kinetics, were observed based on thermogravimetry experiments. The results showed that the reduction and separation efficiency of valuable metals in the carbon-containing pellets were superior to the ones in the previous non-compact mixture. After the reduction roasting of the pellets at 1100 °C and a subsequent magnetic separation, the iron powder with a grade of 91.7 wt % was separated, and in magnetic separation tailings the grades of Nb₂O₅ and (REE)O were beneficiated to approximately twice the grades in the REE–Nb–Fe ore. The reaction rate of the reduction of the carbon-containing pellets was jointly controlled by the carbon gasification reaction and the diffusion of CO in the product layer with an activation energy of 139.26–152.40 kJ·mol⁻¹. Corresponding measures were proposed to further improve the kinetics condition.

Keywords: Bayan Obo; REE–Nb–Fe ore; carbothermal reduction; kinetics

1. Introduction

Bayan Obo ore, Inner Mongolia in China is a well-known multimetallic iron ore deposit, which accounts for 35% of the world's REE reserves and 5.5% of the world's Nb reserves, in addition to abundant iron ore [1]. After a dressing process, most of the Fe (~70%) and a part of REE (<10%) could be recovered [2]. Meanwhile, tailings containing iron oxides, REE oxides ((REE)O) and Nb₂O₅ become a precious secondary resource (~190 million tons). To recover the valuable metals from the tailings, some particular dressing processes have been employed to improve the grade of valuable metals. For example, the grade of Nb₂O₅ was enhanced from 0.14 wt % to ≥3 wt % using a combined dressing process including froth flotation and magnetic separation. However, the grade of REE–Nb–Fe ore beneficiated from the tailings could still not meet the requirements of the Nb industry and REE industry [3]. To separate and recover valuable metals from the low-grade REE–Nb–Fe ore, a process comprising of reduction roasting, magnetic separation, and sulfuric acid (H₂SO₄) leaching was proposed in our previous investigation [4]. In this process, a large quantity of iron was separated from the ore as direct-reduction iron (DRI) via reduction roasting and magnetic separation. The mass fractions of Nb₂O₅ and REE oxides in the magnetic separation tailings

were also significantly increased by these treatments. Subsequently, Nb and REE were recovered in the leaching of the magnetic separation tailings with a H_2SO_4 solution.

In our previous investigation, the REE–Nb–Fe fine ore and pulverized coal were mixed and then roasted in a graphite crucible at an optimal temperature. Although a desirable reduction was obtained, the loading pattern of the non-compact mixture is adverse to industrial production for the following reasons. Firstly, the loosely mixed powders are found to be inconvenient for transporting and feeding. Secondly, the gap between fine ore and pulverized coal enhances the diffusion resistance of the reducing agent, which limits the reduction rate. Thirdly, excess carbon is added to ensure the sufficient reduction reaction of iron oxides. Lastly, the generated dust easily blocks the equipment and contaminates the environment. Overmatching the non-compact mixture, the composite pellets of ore and carbon can be reduced at moderately high temperatures to produce DRI within a rotary hearth furnace (RHF), which has been proven to be environment-friendly and economically viable for the recycling of the industrial wastes which are rich in iron [5,6]. To improve the reduction process, the carbon-containing pellets were prepared through a pressure molding with the mixture of the REE–Nb–Fe fine ore and the pulverized carbon. The reduction and separation efficiency of valuable metals was also evaluated. Following this, the reduction kinetics of the carbon-containing REE–Nb–Fe pellets was studied using thermogravimetry to improve the reduction efficiency in this work.

2. Experimental Section

Table 1 shows the composition of the low-grade REE–Nb–Fe ore which was obtained from Bayan Obo tailings. The pressure-forming pellets were prepared by adding 0.35–0.50 mL water into the uniform mixed powders, which are comprised of REE–Fe–Nb ore powders (6.13 g) with a particle size of <0.096 mm, and graphite powders (0.87 g, $w(C) \geq 99.85\%$) with a particle size of <0.074 mm. A pressure of 30 MPa was applied to the mold via the pressure-forming device, as shown in Figure 1. Finally, the pellets were heated at 110 °C for four hours. Considering the reduction reaction of the iron oxides and the carburization of the iron product, the molar ratio of carbon and oxygen (only in iron oxides) in the pellets is 1.2.

Table 1. Chemical composition of the low-grade REE–Nb–Fe ore (wt %).

T.Fe	FeO	P	F	SiO ₂	CaO	MnO	MgO
44.36	1.35	0.13	2.04	7.17	2.79	0.38	0.6
Na ₂ O	K ₂ O	TiO ₂	Al ₂ O ₃	S	Sc ₂ O ₃	Nb ₂ O ₅	(REE)O
0.85	0.55	5.82	0.21	1.48	0.036	3.04	2.91

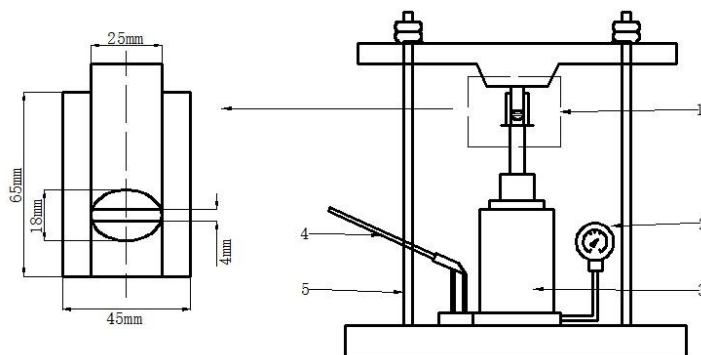


Figure 1. Pressure-forming pellet device (1—Pellet mold; 2—Piezometer; 3—Oil jack; 4—Pressure bar; 5—Pressure support).

The thermogravimetry experiments were carried out in a vertical tube furnace shown in Figure 2, where silicon-molybdenum resistances were used as heating elements. The inner diameter of the furnace tube is $\Phi 50$ mm. The accuracy of the thermo-gravimetric electronic balance is ± 0.1 mg. When the temperature of the heating zone in the furnace reached the desired temperature (950 °C, 1000 °C, 1050 °C, 1100 °C, 1150 °C), the furnace was flushed with nitrogen gas at $4 \text{ L}\cdot\text{min}^{-1}$. Afterwards, the corundum crucible with 3 pellets (21 g) was hung underneath an electronic balance with molybdenum wire. The weight of the samples was recorded at a time interval of 30 s via a computer. It took approximately 300 s for the samples to reach the desired temperature according to the temperature variation measured with Thermocouple II. After the weight data was stabilized for 300 s, the corundum crucible was taken out and cooled via argon gas.

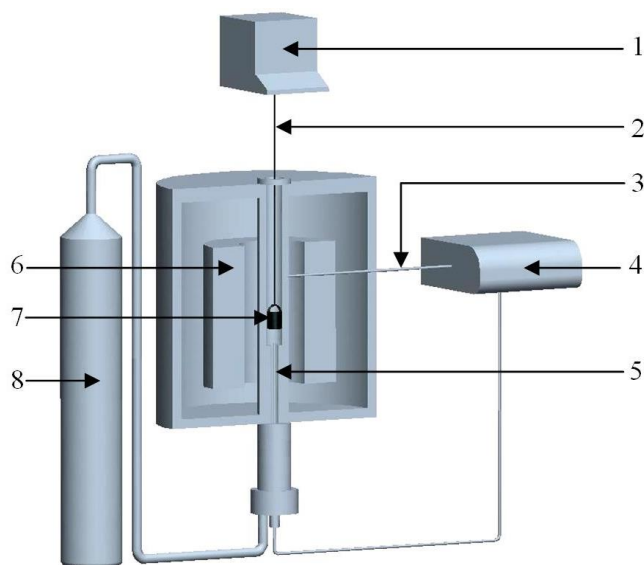


Figure 2. Experimental apparatus of thermogravimetry used in the roasting process (1—Electronic balance; 2—Molybdenum wire; 3—Thermocouple I; 4—Control device; 5—Thermocouple II; 6—Heating element; 7—Graphite basket; 8—Atmosphere control device).

To observe the micrograph of the roasted pellets via scanning electron microscope (SEM), the pellet specimens were mounted in epoxy resin, ground by silicon carbide papers and polished with diamond paste to expose the core cross section. The polished samples were then coated with gold for compositional and microstructural analysis. To separate the Fe from the reduction products, a magnetic separation was carried out in a magnetic tube with a magnetic flux density of 50 mT after milling. The content of Fe in the iron powder magnetically separated from the pellets was determined using the potassium dichromate volumetric method. To measure the content of Nb and REE, the magnetic separation tailing samples were digested with $\text{HNO}_3\text{-HF-HClO}_4$ and analyzed by inductively coupled plasma-optical emission spectrometry (ICP-OES). The detection limit of ICP-OES is $10 \mu\text{g}\cdot\text{L}^{-1}$.

3. Results and Discussion

3.1. Mineral Phase Variation and Separation Efficiency of the Valuable Metals

Figure 3 shows the SEM images of the core cross-section of the roasted pellets at various temperatures. The chemical composition of different positions obtained by energy dispersive spectroscopy (EDS) analysis

is shown in Table 2. There was no apparent metallic iron at 950 °C as the temperature was assumed to be not high enough for thorough carbothermal reduction. The residual carbon content in the pellets was relatively high (as shown at point A), and the greyish white color appeared to be silicate mineral phases (as shown at point B). At 1000 °C, metallic iron was discovered (as shown at point C) which formed a local iron crystal, and pyrochlore ((Ca,Na,Ce)₂(Nb,Ti)₂O₆(F,OH)) (as shown at point D) inlaid in the silicate phase. At 1050 °C and 1100 °C, the reduced iron covered the surface of the ore phase and formed a large area of an iron crystal (as shown at point E and point F). At 1150 °C, the low-melting ore phase with high fluorine content started to melt, slag formed locally (as shown at point G), accompanied by crystallization (as shown at point H), and a large area of iron crystal (as shown at point I) was trapped inside the slag.

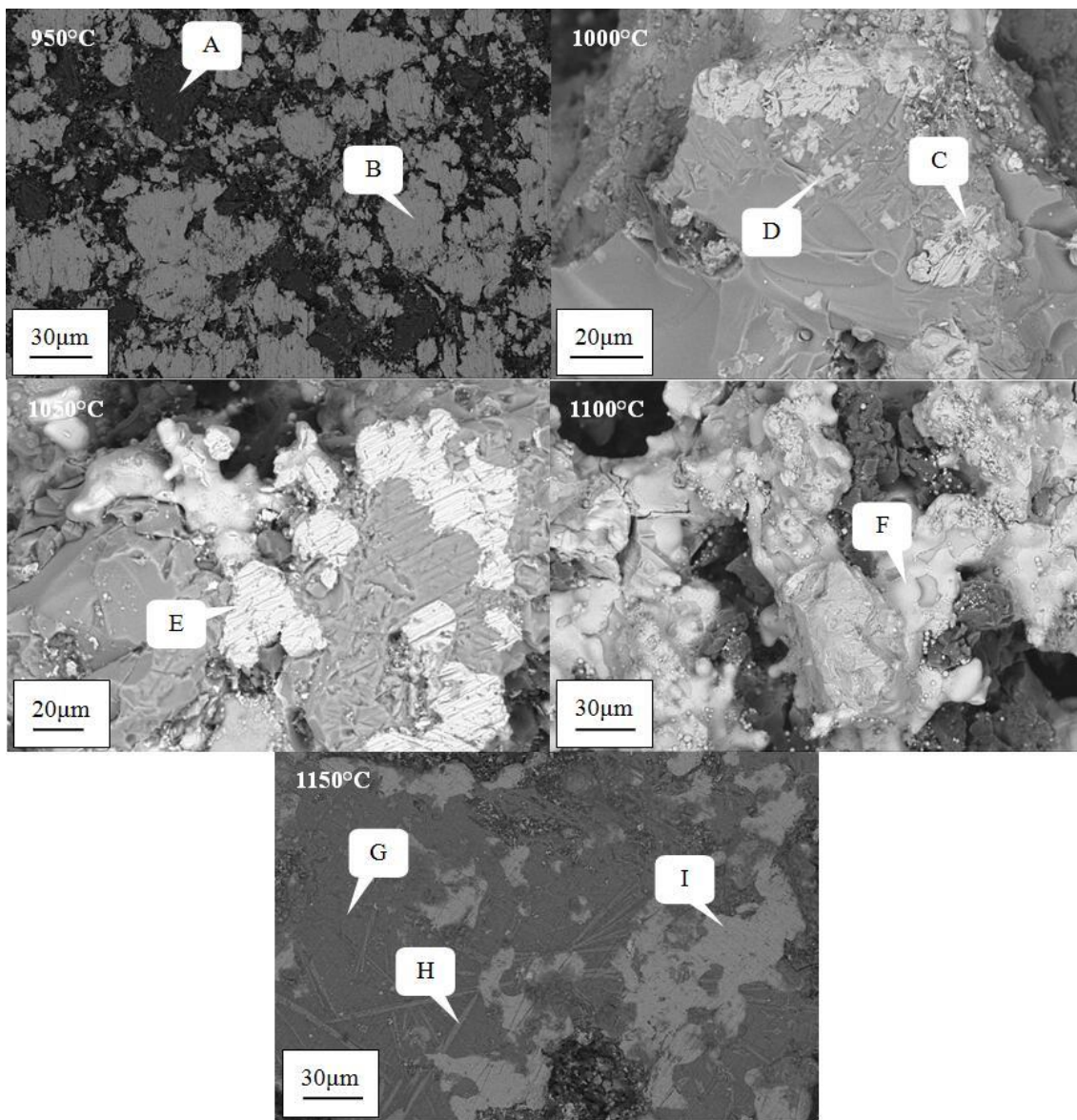


Figure 3. SEM images of the core cross-section of the roasted pellets.

Table 2. EDS results of the characteristic points in the roasted pellets (mass fraction, %).

Analysis Point	C	O	F	Si	Ca	Ti	Fe	Nb	Ce	Nd
A	98.68	-	-	-	-	-	1.32	-	-	-
B	-	27.03	3.23	18.60	10.19	12.89	4.98	8.87	6.44	-
C	11.54	-	-	-	-	-	88.46	-	-	-
D	-	19.29	2.50	0.72	13.61	16.85	4.21	31.85	6.14	4.63
E	7.61	-	-	-	-	-	92.39	-	-	-
F	7.12	-	-	-	-	-	92.88	-	-	-
G	4.45	20.37	22.32	10.52	22.45	7.88	1.88	1.99	3.49	-
H	5.03	31.82	-	9.79	9.47	22.41	1.47	2.41	8.98	4.37
I	7.29	-	-	-	-	-	92.71	-	-	-

After reduction at 1150 °C, a fragmented Nb-enriched region with a particle size smaller than 2 μm can be found around the metallic iron phase. Figure 4 shows the EDS results of the local surface scanning for the reduced pellet at 1150 °C. The green area is metallic iron and Nb enriched in the cavity of the iron phase. The EDS analysis of point J shown in Table 3 shows that the fragments are comprised of niobium and carbon with a small amount of titanium and iron. It was further deduced that the fragments are NbC through a comparison between the XRD patterns of magnetic separation tailings after reduction at 1150 °C and pure NbC, using the data of PDF-65-7964., as shown in Figure 5.

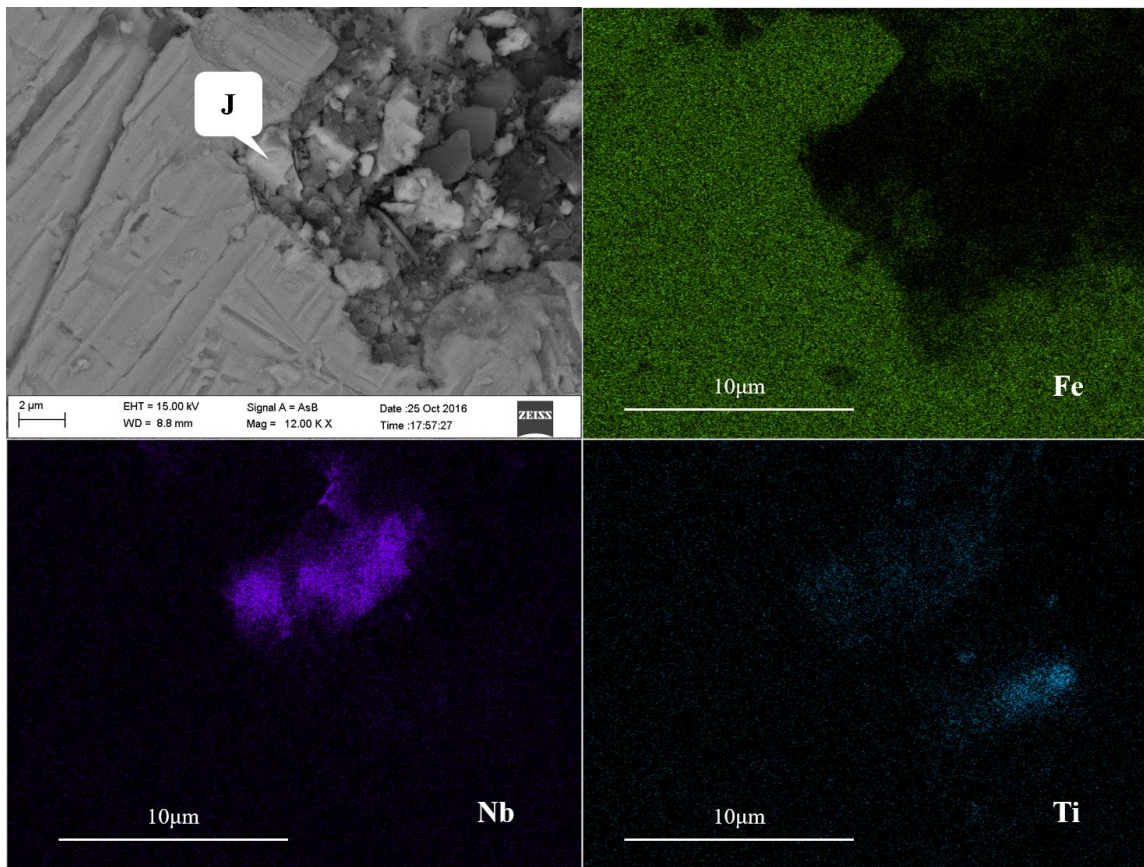


Figure 4. EDS results of the local surface scanning for the reduced pellet at 1150 °C.

Table 3. EDS results of point “J” in the reduced pellet at 1150 °C.

Analysis Point	C	Ti	Fe	Nb
J	18.11	2.63	2.64	76.62

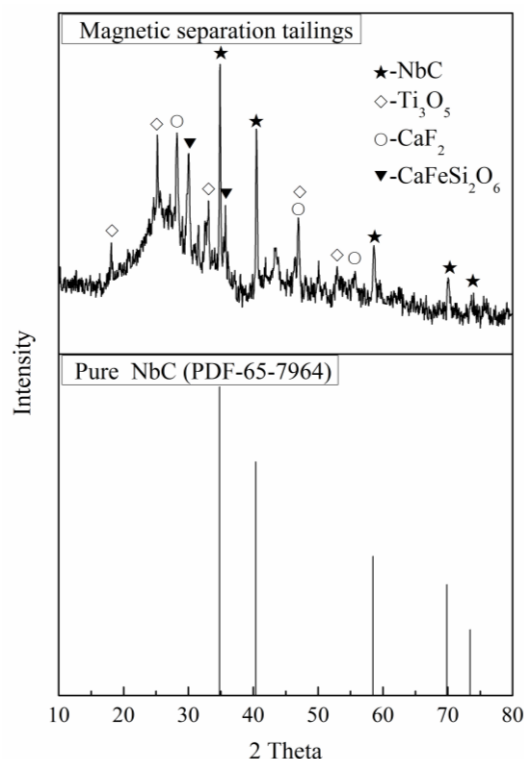
**Figure 5.** A comparison between the XRD patterns of the magnetic separation tailings and pure NbC.

Figure 6 shows the relationship between the temperature and the Gibbs free energy change of the carbothermal reduction reaction of niobium oxides under the standard conditions. The Gibbs free energy changes of the reactions in Figure 6 were obtained by calculation in virtue of the thermodynamic data in reference [7]. According to Figure 6, the reduction process of niobium oxides follows the sequence of $\text{Nb}_2\text{O}_5 \rightarrow \text{NbO}_2 \rightarrow \text{NbC}$, which has been confirmed by Shimada et al. through their carbothermal reduction experiments [8]. Firstly, Nb_2O_5 was reduced to NbO_2 , and the skip-level reduction reaction from Nb_2O_5 to NbO , with a higher Gibbs free energy change, is demonstrated to be inexistent. Then, NbO_2 was reduced to NbC instead of NbO , because the Gibbs free energy change of NbC formed by the carbothermal reduction of NbO_2 is apparently lower than that of the NbO formation from NbO_2 . According to the experimental results, NbC formed through the reduction of niobium oxide in the reduction of the carbon pellets in the REE–Nb–Fe ore at 1150 °C. Since NbC is insoluble in inorganic acids, NbC generated during the reductive roasting process could not be leached efficiently during the subsequent sulfuric acid leaching process, which affects the recovery efficiency of Nb. Therefore, the reduction temperature of carbon pellets in the REE–Nb–Fe ore should be less than 1150 °C in order to avoid the formation of NbC .

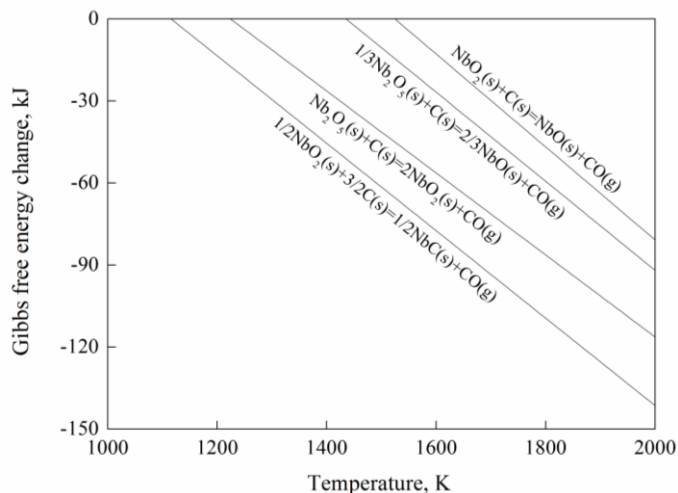


Figure 6. The relationship between the temperature and Gibbs free energy change of the carbothermal reduction reaction of niobium oxides.

Figure 7 shows the grade and the recovery of Fe in the iron powder magnetically separated from the carbon-containing pellets and in the non-compact mixture after reduction roasting, respectively. Compared to the non-compact mixture, the loading pattern of pressure-forming pellets increases the separation efficiency of Fe, including the grade and the recovery, naturally. The grade and recovery both increase with the increasing temperature. Meanwhile, niobium and rare earth elements were better beneficiated in the magnetic separation tailings. As shown in Figure 8, the grades of Nb₂O₅ and (REE)O in the magnetic separation tailings from pressure-forming pellets are higher than the ones from the non-compact mixture due to the higher separation efficiency of Fe and the lesser amount of unreacted carbon. In the carbon-containing pellets, the lower carbon addition leads to less unreacted carbon after reduction roasting. After the reduction roasting of the pellets at 1100 °C and the magnetic separation, the iron powder with a grade of 91.7 wt % was obtained, and the grades of Nb₂O₅ and (REE)O in the magnetic separation tailings were beneficiated to 6.06 wt % and 5.87 wt %, approximately twice the grades in REE–Nb–Fe ore, respectively.

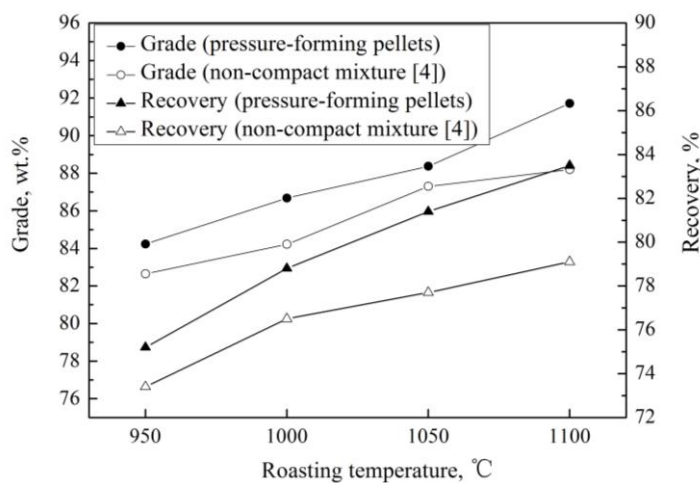


Figure 7. Grade and recovery of Fe in the iron powder.

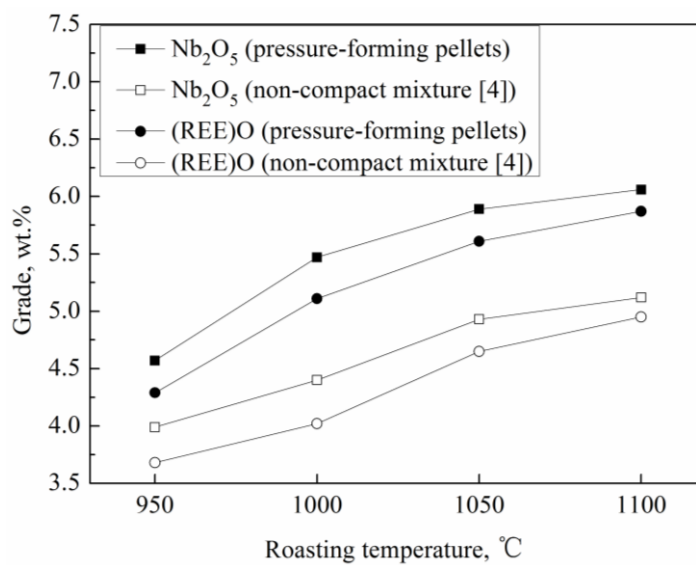


Figure 8. Grades of Nb₂O₅ and (REE)O in the magnetic separation tailings.

3.2. Reduction Degree at Different Temperature

It was shown in our previous work [4] that, at ≤ 1100 °C, iron oxide is the sole metallic oxide in REE–Nb–Fe ore which can be reduced by carbon. At the initial stage of the roasting process, REE–Fe–Nb ore particles contacted with graphite particles directly. So iron oxides were reduced by carbon, shown as Equations (1)–(3). With the generation of CO, iron oxide can be further reduced by CO which is shown as Equations (4)–(6). Following this, the gasification reaction of carbon (Boudouard reaction) happens, shown as Equation (7) [9]. Man et al. investigated the Boudouard reaction kinetics using the thermogravimetric method at a constant heating rate; the rate of the Boudouard reaction increases significantly at >920 °C [10]. Meanwhile, the generation of metallic iron on the surface of the ore particles isolates the iron oxides and graphite particles. Therefore, CO replaces C as the actual reductant by diffusion through the iron product layer at high temperature [11]. We can obtain Equation (8) by summing Equations (4)–(7). Therefore, the weight loss of the carbon-containing pellets becomes the weight loss of the carbothermal reduction of iron oxides. Based on the weight-loss method, the reaction fraction, f , which represents the reduction degree of iron oxides can be calculated using Equation (9) [11].



$$f = \frac{\Delta W_t}{\Delta W_{\max}} = \frac{(W_0 - W_t)}{W_0 \cdot \frac{M_{\text{CO}}}{M_{\text{O}}}} \times 100\% \quad (9)$$

where, f is the reaction fraction, ΔW_t is the weight loss at the time of t (g), ΔW_{\max} is the maximum theoretical reduction weight loss (g), W_0 is the initial weight of the pellets (g), W_t is the weight of the pellets at the time of t (g), W_{O} is the oxygen weight of the iron oxides in the pellets (g), M_{CO} is the molar mass of the carbon monoxide ($\text{g}\cdot\text{mol}^{-1}$), and M_{O} is the molar mass of the oxygen ($\text{g}\cdot\text{mol}^{-1}$).

The changes in the reaction fraction in the roasting process are shown in Figure 9. If all of the iron oxides were reduced to metallic iron, the weight loss of the pellets should reach the expected maximum weight loss ($\Delta W_t = \Delta W_{\max} = 6.09$ g), and f should be 100%. However, the maximum value of f in the roasting process is 92.6% at 1100 °C, as shown in Figure 9, which means the iron oxides cannot be thoroughly reduced to metallic iron. Moreover, the reduction reaction rate increases significantly with the increasing temperature. At 1100 °C, the reduction degree reaches >90% within 30 min, which is far less than the reaction time (180 min) required in our previous work with the loading pattern of the non-compact mixture. Hence, the reaction efficiency vastly improves using carbon-containing pellets.

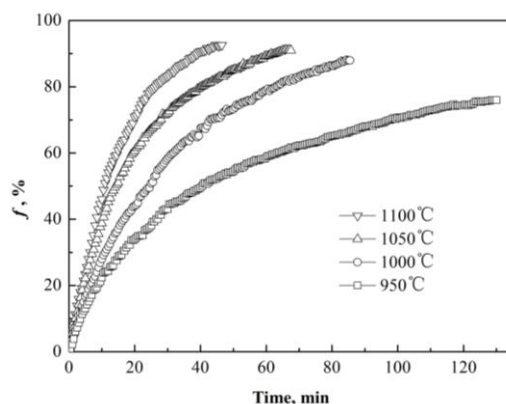


Figure 9. Variation of reaction fraction at different times in the roasting process.

3.3. Kinetic Analysis of Reduction Reaction

As stated in Section 3.1, the reduced iron covered the surface of the unreacted ore and formed a large area of iron crystal. Thus the reduction reaction process of the particles in the carbon-containing pellet can be described via the shrinking unreacted core model, as shown in Figure 10. The carbothermal reduction process includes the following:

- The gasification reaction of carbon;
- The external diffusion of CO/CO_2 through the gas phase boundary layer;
- The internal diffusion of CO/CO_2 through the iron product layer;
- The interfacial reduction reaction of iron oxide particles.

It is generally recognized that the diffusion of CO/CO_2 through the gas phase boundary layer is too fast to become the restrictive link of the reduction rate at a high temperature [12]. To discuss the kinetics of the reduction reaction, we assumed that (1) the pellet was isotropic, and that the ore particles and the carbon particles uniformly distributed; (2) the temperature gradient and gas phase concentration gradient were negligible; and (3) the temperature change of the pellets at the initial stage (~ 300 s) was insignificant. According to the above analysis and assumption, the reduction reaction kinetics can be described by three

models according to the restrictive links of rate, as shown in Table 4, where, f is the reaction fraction until time t , k is the apparent reaction rate constant (s^{-1}), and t is the reaction time (s).

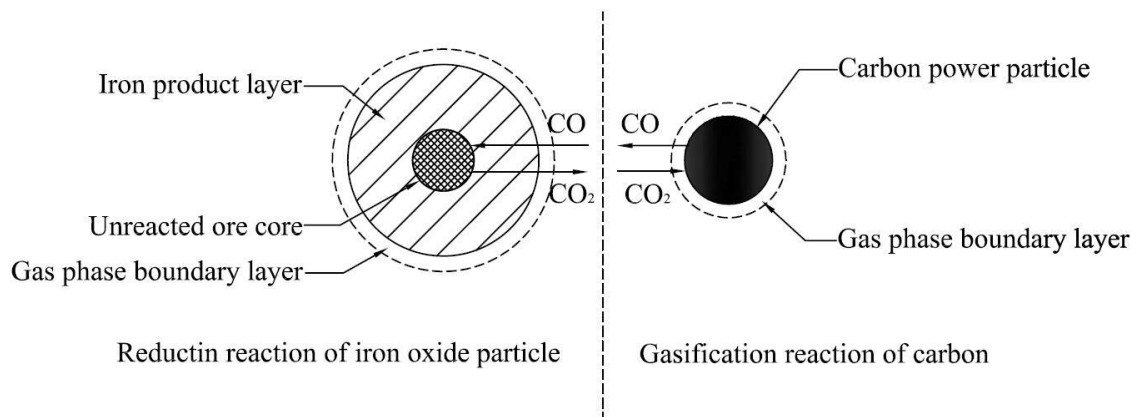


Figure 10. Schematic diagram of the reduction reaction process.

Table 4. Kinetics models of the reduction reaction.

Model	Restrictive Link of Reaction Rate	Equation	No.	References
I	Gasification reaction of carbon	$-\ln(1 - f) = kt$	(10)	[13]
II	Interface reaction between CO and iron oxides	$1 - (1 - f)^{1/3} = kt$	(11)	[14]
III	Diffusion of CO in product layer	$1 - 2/3f - (1 - f)^{2/3} = kt$	(12)	[15]

As shown in Figure 11, the data of $-\ln(1 - f)$, $1 - (1 - f)^{1/3}$ and $1 - 2/3f - (1 - f)^{2/3}$ at different times in the roasting process was calculated according to Equations (10)–(12) in Table 4 and then linearly fitted, and the rate constant k , equal to the slope of the fitted line, was obtained. The rate constant k and the correlation coefficient R^2 of the linear fitting are listed in Table 5. As can be seen, Model I and Model III have good linear relations with time t , whose correlation coefficients are higher than those of Model II. Hence, it can be predicted that the reaction kinetics may be governed by the gasification reaction of carbon or by the diffusion of CO/CO₂ in the product layer.

To determine the restrictive link of the reaction rate further, the apparent energy was calculated based on the Arrhenius equation, Equation (13).

$$\ln k = \ln A - \frac{E}{RT} \tag{13}$$

where, A is the frequency factor, E is the apparent activation energy ($J \cdot mol^{-1}$), and R is the gas constant, $8.314 (J \cdot mol^{-1} \cdot K^{-1})$.

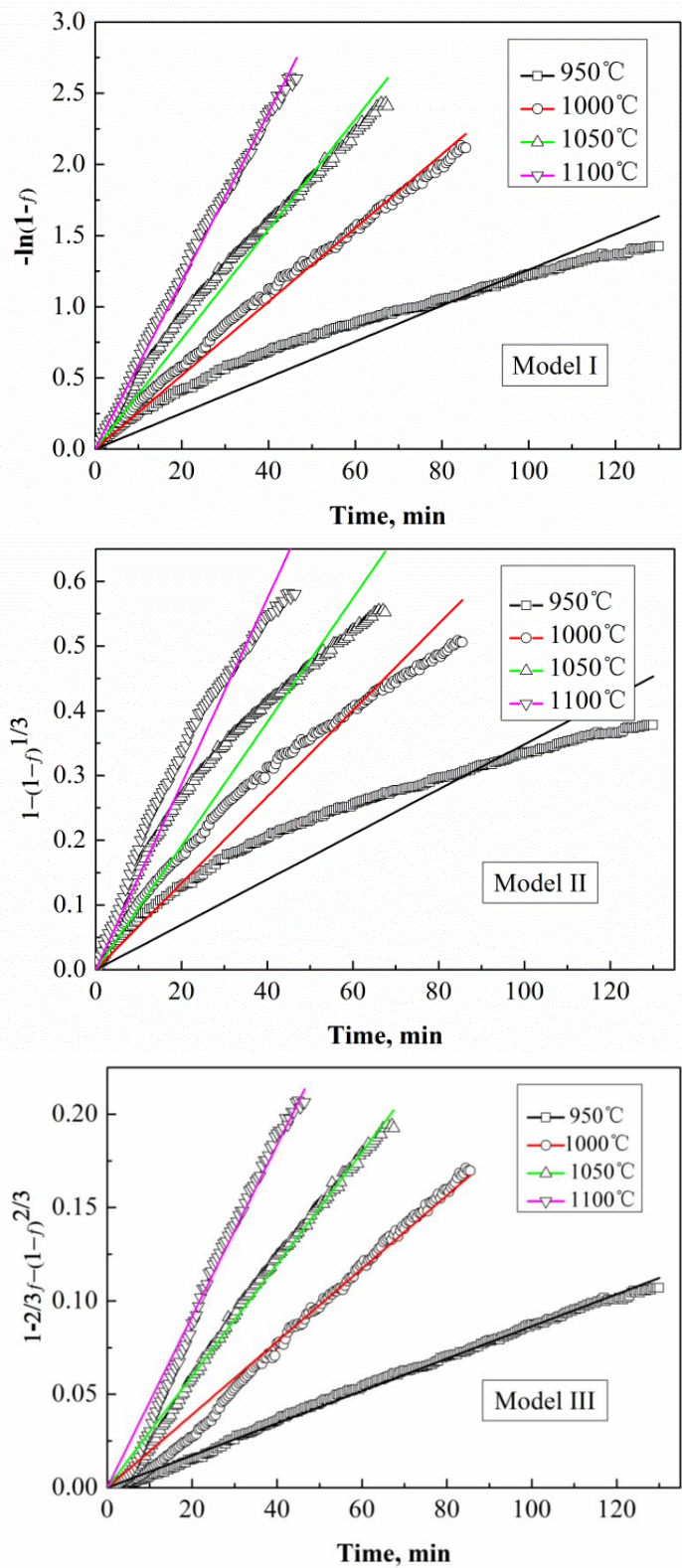
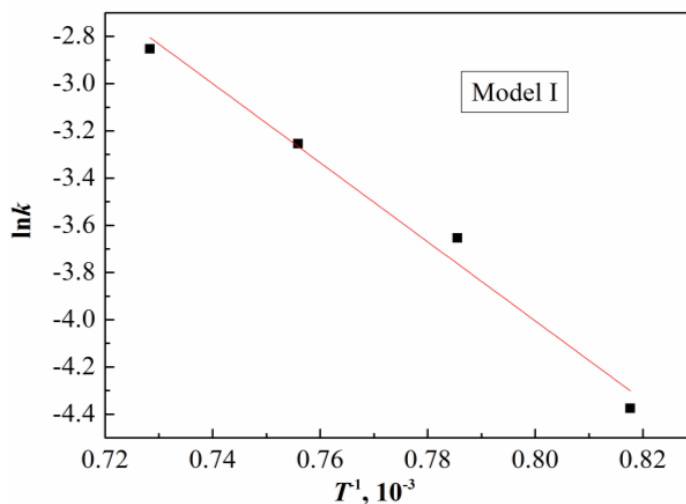


Figure 11. Linear fitting of different kinetics models.

Table 5. Calculated parameters of the linear fitting.

Model	Temperature, °C	Time, min	k, s^{-1}	R^2
I	950	0~129	1.26×10^{-2}	0.9822
	1000	0~85	2.59×10^{-2}	0.9977
	1050	0~67	3.86×10^{-2}	0.9952
	1100	0~46	5.91×10^{-2}	0.9992
II	950	0~129	3.48×10^{-3}	0.9700
	1000	0~85	6.68×10^{-3}	0.9880
	1050	0~67	9.56×10^{-3}	0.9807
	1100	0~46	1.43×10^{-2}	0.9894
III	950	0~129	8.64×10^{-4}	0.9991
	1000	0~85	1.96×10^{-3}	0.9961
	1050	0~67	2.99×10^{-3}	0.9985
	1100	0~46	4.59×10^{-3}	0.9952

In theory, there is a linear relation between $\ln k$ and T^{-1} . Therefore E and A can be obtained from the slope and intercept of the line fitted with $\ln k$ and T^{-1} , as shown in Figure 12. The activation energy E is found, for Model I and Model III, to be $139.26 \text{ kJ}\cdot\text{mol}^{-1}$ and $152.40 \text{ kJ}\cdot\text{mol}^{-1}$, while the frequency factor A is 12,027.01 and 3064.19 for Model I and Model III respectively. Walker et al. [16] recommended $360 \text{ kJ}\cdot\text{mol}^{-1}$ as the true activation energy for the reaction of carbon with dioxide, and the approximate values of the activation energy were obtained by Rao [14] ($301 \text{ kJ}\cdot\text{mol}^{-1}$) and Fruhen [17] ($293\text{--}335 \text{ kJ}\cdot\text{mol}^{-1}$). It has also been said that the apparent activation energy is about half of the true value when the reaction is controlled by both pore diffusion and chemical reaction [16]. Consequently, the reaction kinetics of the carbon-containing pellets in our work are co-controlled by the carbon gasification reaction and the diffusion of CO in the product layer, according to the activation energy at $139.26\text{--}152.40 \text{ kJ}\cdot\text{mol}^{-1}$.

**Figure 12.** Cont.

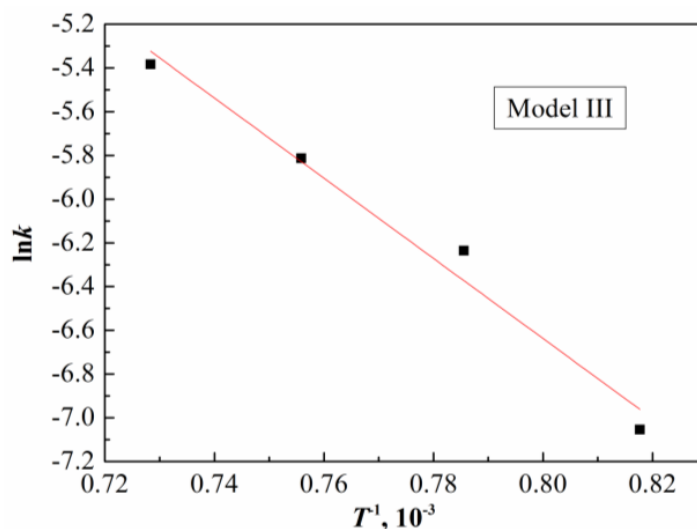


Figure 12. Relationship between $\ln k$ and T^{-1} for Model I and Model III.

To improve the reduction kinetics of carbon-containing pellets, two methods can be applied: (1) instead of graphite powders, choosing carbonaceous powders with higher activity such as coal, coke, semi-coke, etc. as the reductant; (2) grinding the ore powders to a finer granularity to restrict the thickness of the product layer and to reduce the diffusion resistance.

3.4. Process Flow

Based on the above observations, a modified process can be proposed, as presented in Figure 13. Firstly, the low grade REE–Nb–Fe ore and carbonaceous powders, such as coal, coke, semi-coke, etc., were finely grinded, homogeneously mixed and pressure-forming briquetted into the carbon-containing pellets. Secondly, the reduction roasting of the pellets was carried out within a rotary hearth furnace at 1100 °C, and the metallized pellets were obtained. Then, the metallized pellets were smashed and magnetically separated. Finally, the iron powders with a high grade (>90%) and recovery rate (>80%) were obtained, and Nb₂O₅ and (REE)O were beneficiated into the magnetic separation tailings with approximately twice the grades of REE–Nb–Fe ore. Subsequently, Nb and REE can be extracted from the magnetic separation tailings using a hydro-metallurgical method, such as the aforementioned H₂SO₄ leaching process, or another pyro-metallurgical method. Compared to the non-compact mixture, the loading pattern of the pressure-forming pellets is convenient for transporting and feeding, and the roasting reduction of the carbon-containing pellets in RHF is highly efficient, economical, and environment-friendly.

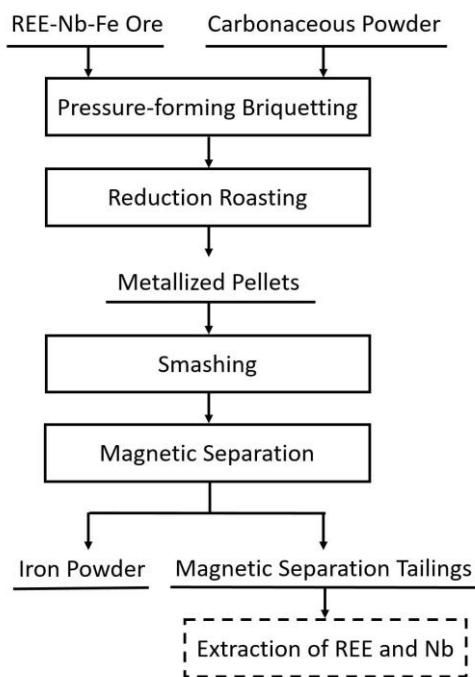


Figure 13. Flow sheet of the modified process.

4. Conclusions

To adapt to the requirement of industrial production and improve the reduction efficiency, the carbon-containing REE–Nb–Fe ore pellets were prepared through a pressure molding to replace the non-compact mixture used in our previous work. The mineral phase variation and separation efficiency of valuable metals was evaluated. The carbothermal reduction kinetics of the pellets was studied using thermogravimetry.

The separation efficiency of valuable metals in the carbon-containing pellets was superior to that of the ones in the previous non-compact mixture. After the reduction roasting of the pellets at 1100 °C and after a magnetic separation, the iron powder with a grade of 91.7 wt % was separated. The grades of Nb₂O₅ and (REE)O in magnetic separation tailings were beneficiated to 6.06 wt % and 5.87 wt %, respectively, approximately twice the grades in REE–Nb–Fe ore. The reduction kinetics of the carbon-containing pellets were jointly controlled by the carbon gasification reaction and the diffusion of CO in the product layer, with an activation energy of 139.26–152.40 kJ·mol^{−1}. The carbonaceous powders with a higher activity and the ore powders with a finer granularity were proposed to improve the reduction kinetics of carbon-containing REE–Nb–Fe ore.

Acknowledgments: Financial support to this project is provided by the National Natural Science Foundation of China (Grant No. 51774087), the National Key R & D Program of China (Grant No. 2017YFC0805100), the Fundamental Research Funds for the Central Universities (Grant No. N162504015), the China Scholarship Council (Grant No. 201706085022).

Author Contributions: Bo Zhang and Chengjun Liu conceived and designed the experiments; Bo Zhang and Yun Ye performed the experiments; Bo Zhang analyzed the data; Maofa Jiang contributed reagents/materials/analysis tools; Bo Zhang and Yong Fan made the figures and tables and wrote the paper.

Conflicts of Interest: The authors declare no conflict of interest.

References

1. Ding, Y.G.; Xue, Q.G.; Wang, G.; Wang, J.S. Recovery behavior of rare earth from Bayan Obo complex iron ore. *Metall. Mater. Trans. B* **2013**, *44*, 28–36. [[CrossRef](#)]
2. Li, J.C.; Guo, Z.C. Innovative methodology to enrich britholite ($\text{Ca}_3\text{Ce}_2[(\text{Si,P})\text{O}_4]_3\text{F}$) phase from rare-earth-rich slag by super gravity. *Metall. Mater. Trans. B* **2014**, *45*, 1272–1280. [[CrossRef](#)]
3. Gibson, C.E.; Kelebek, S.; Aghamirian, M. Niobium oxide mineral flotation: A review of relevant literature and the current state of industrial operations. *Int. J. Miner. Process.* **2015**, *137*, 82–97. [[CrossRef](#)]
4. Zhang, B.; Liu, C.J.; Li, C.L.; Jiang, M.F. Separation and recovery of valuable metals from low-grade REE–Nb–Fe ore. *Int. J. Miner. Process.* **2016**, *150*, 16–23. [[CrossRef](#)]
5. Lee, Y.S.; Ri, D.W.; Yi, S.H.; Sohn, I. Relationship between the reduction degree and strength of DRI pellets produced from iron and carbon bearing wastes using an RHF simulator. *ISIJ Int.* **2012**, *52*, 1454–1462. [[CrossRef](#)]
6. Lu, W.K.; Huang, D.F. The evolution of ironmaking process based on coal-containing iron ore agglomerates. *ISIJ Int.* **2001**, *41*, 807–812. [[CrossRef](#)]
7. Barin, I.; Knacke, O.; Kubaschewski, O. *Thermochemical Properties of Inorganic Substances*; Springer-Verlag: Berlin, Germany, 1977.
8. Shimada, S.; Koyama, T.; Kodaira, K.; Mastushita, T. Formation of NbC and TaC by solid-state reaction. *J. Mater. Sci.* **1983**, *18*, 1291–1296. [[CrossRef](#)]
9. Tiwari, P.; Bandyopadhyay, D.; Ghosh, A. Kinetics of gasification of carbon and carbothermal reduction of iron oxide. *Ironmak. Steelmak.* **1992**, *19*, 464–468.
10. Man, Y. A Study on the Direct Reduction Characteristics of Iron Ore-Coal Composite Pellets under Gas-Solid Base. Ph.D. Thesis, University of Science and Technology Beijing, Beijing, China, 30 October 2014. (In Chinese)
11. Wang, Q.; Yang, Z.; Tian, J.; Li, W.; Sun, J. Mechanisms of reduction in iron ore coal composite pellet. *Steel Res.* **1997**, *24*, 457–460.
12. Man, Y.; Feng, J.X.; Li, F.J.; Ge, Q.; Chen, Y.M.; Zhou, J.Z. Influence of temperature and time on reduction behavior in iron ore-coal composite pellets. *Powder Technol.* **2014**, *256*, 361–366. [[CrossRef](#)]
13. Seaton, C.E.; Foster, J.S.; Velasco, J. Reduction kinetics of hematite and magnetite pellets containing coal char. *Trans. Iron Steel Inst. Jpn* **1983**, *23*, 490–496. [[CrossRef](#)]
14. Rao, Y.K. The kinetics of reduction of hematite by carbon. *Metall. Trans.* **1971**, *2*, 1439–1447.
15. Ginstling, A.M.; Brownstein, V.I. Concerning the diffusion kinetics of reaction in spherical particles. *J. Appl. Chem. USSR* **1950**, *23*, 1327–1338.
16. Eley, D.D.; Selwood, P.W.; Weisz, P.B. *Advances in Catalysis, Volume XI*; Academic Press: New York, NY, USA, 1959; pp. 134–217.
17. Fruhen, R.J. The rate of reduction of iron oxides by carbon. *Metall. Mater. Trans. B* **1977**, *8*, 175–178. [[CrossRef](#)]



© 2018 by the authors. Licensee MDPI, Basel, Switzerland. This article is an open access article distributed under the terms and conditions of the Creative Commons Attribution (CC BY) license (<http://creativecommons.org/licenses/by/4.0/>).